Supplementary Figures and Tables

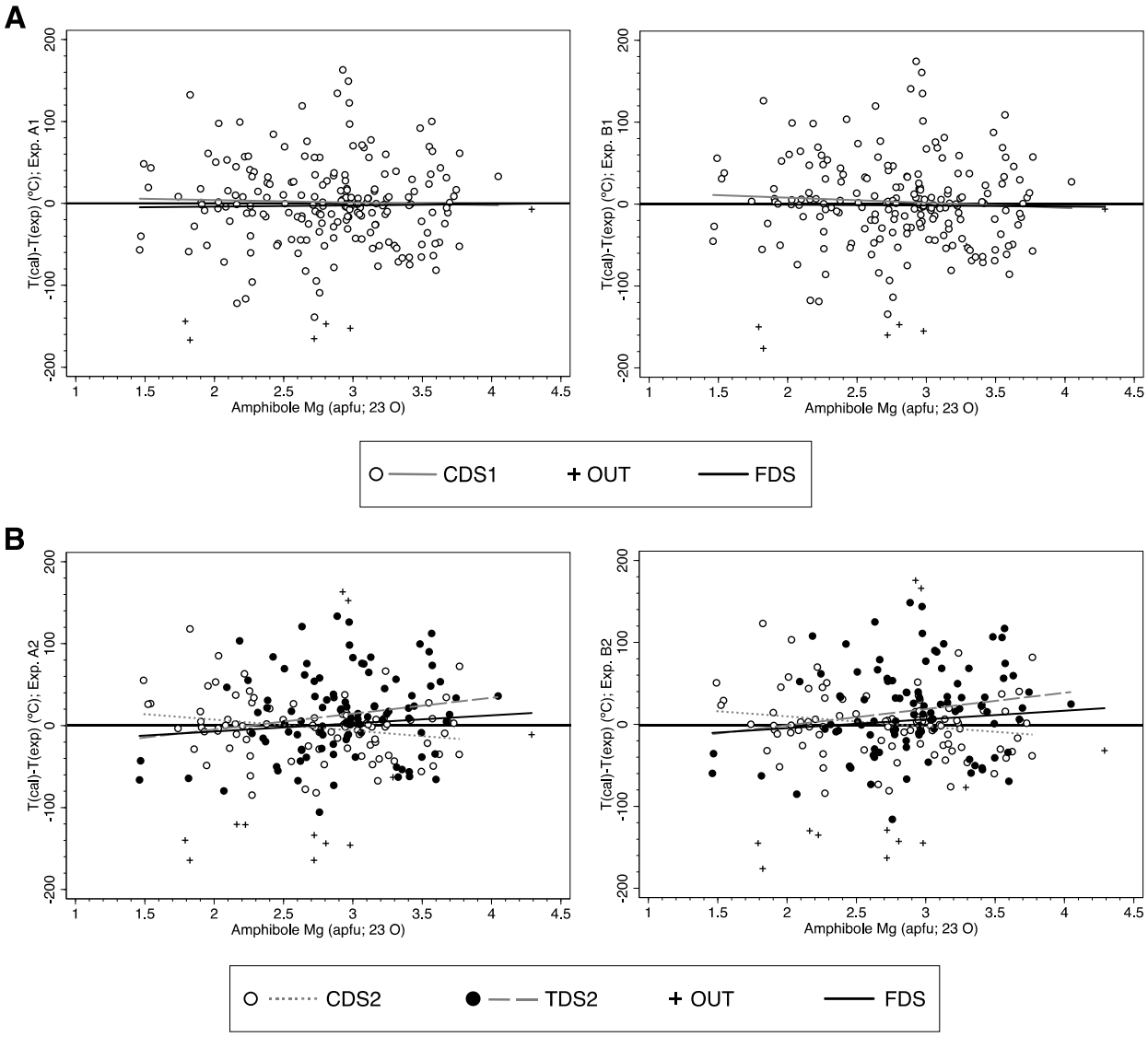

Fig. 1SB. Relationships of residuals versus amphibole Mg occupancy for the new amphibole-plagioclase NaSi–CaAl exchange thermometers. A) Expressions A1 and B1. B) Expressions A2 and B2. Abbreviations: CDS1, Calibration Data Set 1; CDS2, Calibration Data Set 2; TDS2, Test Data Set 2; FDS, Full Data Set; OUT, outliers.

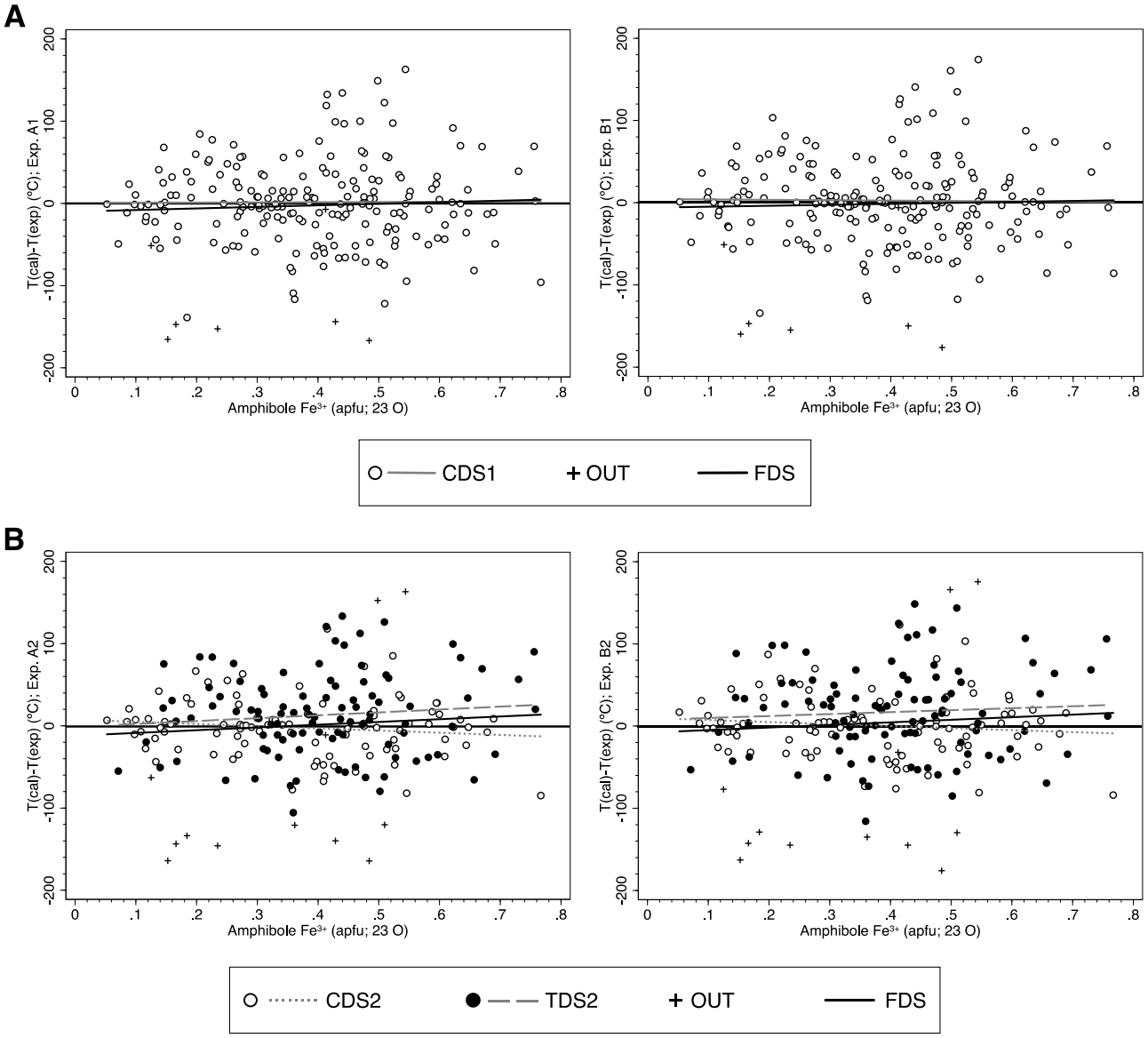

Fig. 2SB. Relationships of residuals versus amphibole Fe^{3+} occupancy for the new amphibole-plagioclase NaSi–CaAl exchange thermometers. A) Expressions A1 and B1. B) Expressions A2 and B2. Abbreviations: CDS1, Calibration Data Set 1; CDS2, Calibration Data Set 2; TDS2, Test Data Set 2; FDS, Full Data Set; OUT, outliers.

Table 1SB. Ranges of pressure, temperature and compositional variables of the full amphibole-plagioclase data set (203 observations)

FDS parameters	*Amphibole composition (apfu, 23O)*	*Amphibole phase components*
P(kbar)=1—15	*Si=5.956—7.431*	p_1*=0.034—0.214*
T(ºC)=640—1000ºC	*Ti=0.004—0.349*	p_2*=-0.277— 0.311*
lnK^{id}*=-9.00— -1.99*	*Al=0.668—3.392*	p_3*=0.002—0.174*
$RTlnK^{id}$*=-*76905*— -17741 (J)*	*Fe =0.655—3.110*	p_4*=0.026—0.383*
lnK^{id}*=-9.00— -1.99*	*Mg=1.461—4.289*	p_5*=0.023—0.708*
Den(A1)=-182—-122	*Ca=1.287—1.868*	p_1*=0.034—0.214*
Den(B1)=-183— -124	*Na=0.229—0.785*	p_2*=-0.277— 0.311*
Den(A2)=-195— -132	*K<0.223*	p_3*=0.002—0.174*
Den(B2)=-194— -132	*F<0.062*	p_4*=0.026—0.383*
Plagioclase phase components	*Cl<0.006*	p_5*=0.023—0.708*
p_{ab}*=0.108—0.820*	Al_{VI}*=0.093—1.449*	p_6*<0.223*
p_{an}*=0.180—0.891*	Na_{M4}*=0.067—0.427*	p_7*=0.006—0.183*
p_{or}*<0.109*	Na_A*= 0.023—0.708*	p_8*=0.029—0.345*
	Fe^{2+}*=0.285—2.676*	p_9*=-0.215—0.321*
	Fe^{3+}*=0.052—0.767*	p_{10}*<0.053*
	Mg/(Mg+Fe^{2+}*)=0.353—0.928*	p_{11}*<0.050*
	Fe^{3+}/Fe_T *=0.039 —0.699*	

Table 2SB. Test of the new amphibole-plagioclase NaSi–CaAl exchange thermometric expressions. Testing model[1]: $\hat{T}_i = a + b\,T_i$

Expression	*A1*	*A1*	*B1*	*B1*	*A2*	*A2*	*A2*	*B2*	*B2*	*B2*
Data set[2]	*CDS1*	*FDS*	*CDS1*	*FDS*	*CDS2*	*TDS2*	*FDS*	*CDS2*	*TDS2*	*FDS*
Observations	196	203	196	203	92	99	203	92	99	203
R-squared	0.99	0.99	0.74	0.69	0.99	0.99	0.99	0.99	0.99	0.99
RMSE (ºC)	50	55	49	54	35	51	55	36	52	56
AAD (ºC)	37	40	37	40	26	42	39	26	42	40
MAD (ºC)	27	29	28	30	18	35	29	21	35	28
Slope, b	1.000 ±0.004 t=250	0.995 ±0.005 t=199	0.85 ±0.04 t=21.3	0.84 ±0.04 t=21	0.996 ±0.004 t=249	1.014 ±0.006 t=169	1.000 ±0.005 t=200	0.998 ±0.005 t=200	1.013 ±0.006 t=169	0.999 ±0.005 t=200
Intercept, a	0	0	124 ±31 t=4.0	135 ±33 t= 4.1	0	0	0	0	0	0

Notes: 1, non-constant regression model used when $P(>|t|) > 0$ for a parameter in model $\hat{T}_i = a + b\,T_i$. 2: CDS1, Calibration Data Set 1, for expressions A1 and B1 (i.e., full data set excluding 7 outliers); CDS2, Calibration Data Set 2, for expressions A2 and B2; FDS, Full Data Set; TDS2, Test Data Set 2, for expression A2 and B2.
Other abbreviations: AAD, Average Absolute Deviation; MAD, Median Absolute Deviation; RMSE, Root-Mean-Square Error.

Table 3SB. Test of the amphibole-plagioclase NaSi–CaAl exchange thermometer from Holland and Blundy (1994): expression B. Testing model[1]: $\hat{T}_i = a + b\,T_i$

Data set[2]	*FDS*	*FDS*	*CDS2*	*CDS2*	*TDS2*	*TDS2*
Temperature range[3]	*FTR*	*CTR*	*FTR*	*CTR*	*FTR*	*CTR*
Observations	201	158	91	70	98	76
R-squared	0.52	0.40	0.64	0.60	0.46	0.99
RMSE (ºC)	60	61	52	51	67	72
AAD (ºC)	56	53	48	42	60	58
MAD (ºC)	42	41	37	35	49	49
Slope, b	0.660±0.045 t = 15	0.643±0.063 t = 10	0.665±0.053 t = 13	0.711±0.070 t = 10	0.674±0.075 t = 9.0	0.970±0.010 t = 97
Intercept, a	255±37 t = 6.9	268±50 t = 5.4	261±45 t = 5.8	226±56 t = 4.0	239±62 t = 3.9	0

Notes: 1, non-constant regression model used when $P(>|t|) > 0$ for a parameter in model $\hat{T}_i = a + b\,T_i$. 2: CDS2, Calibration Data Set 2; FDS, Full Data Set; TDS2, Test Data Set 2. 3: CTR, Calibration Temperature Range; FTR, Full Temperature Range.
Other abbreviations: AAD, Average Absolute Deviation; MAD, Median Absolute Deviation; RMSE, Root-Mean-Square Error.

Table 4SB. Test of the amphibole-only thermometer from Ridolfi and Renzulli (2012): expression 2. Testing model[1]: $\hat{T}_i = a + b\,T_i$

Data set[2]	*FDS*	*FDS*	*CDS2*	*CDS2*	*TDS2*	*TDS2*
Temperature range[3]	*FTR*	*CTR*	*FTR*	*CTR*	*FTR*	*CTR*
Observations	166	123	84	60	75	57
R-squared	0.39	0.25	0.47	0.16	0.41	0.48
RMSE (ºC)	51	44	51	42	43	33
AAD (ºC)	65	45	79	59	51	33
MAD (ºC)	49	36	67	54	34	25
Slope, b	0.436±0.043 t = 10	0.461±0.072 t = 6.4	0.489±0.057 t = 8.6	0.33±0.10 t = 3.3	0.407±0.057 t = 7.1	0.526±0.073 t = 7.2
Intercept, a	520±36 t = 14	499±63 t = 7.9	495±48 t = 10	641±89 t =7.2	527±48 t = 11	421±65 t = 6.5

Notes: 1, non-constant regression model used when $P(>|t|) > 0$ for a parameter in model $\hat{T}_i = a + b\,T_i$. 2: CDS2, Calibration Data Set 2; FDS, Full Data Set; TDS2, Test Data Set 2. 3: CTR, Calibration Temperature Range; FTR, Full Temperature Range.
Other abbreviations: AAD, Average Absolute Deviation; MAD, Median Absolute Deviation; RMSE, Root-Mean-Square Error.

Table 5SB. Test of the amphibole-only thermometer from Putirka (2016): expression 5. Testing model[1]: $\hat{T}_i = a + b\,T_i$

Data set[2]	*FDS*	*FDS*	*CDS2*	*CDS2*	*TDS2*	*TDS2*
Temperature range[3]	*FTR*	*CTR*	*FTR*	*CTR*	*FTR*	*CTR*
Observations	152	132	65	52	76	70
R-squared	0.35	0.47	0.33	0.38	0.52	0.61
RMSE (ºC)	52	48	46	41	48	43
AAD (ºC)	60	45	83	62	41	34
MAD (ºC)	41	35	59	50	30	26
Slope, b	0.412±0.046 t = 9.0	0.563±0.053 t = 11	0.295±0.053 t = 5.6	0.358±0.065 t = 5.5	0.605±0.067 t = 9.0	0.749±0.072 t = 10
Intercept, a	513±37 t = 14	382±44 t = 8.7	632±44 t = 14	578±55 t = 11	341±55 t = 6.2	218±59 t = 3.7

Notes: 1, non-constant regression model used when $P(>|t|) > 0$ for a parameter in model $\hat{T}_i = a + b\,T_i$. 2: CDS2, Calibration Data Set 2; FDS, Full Data Set; TDS2, Test Data Set 2. 3: CTR, Calibration Temperature Range; FTR, Full Temperature Range.
Other abbreviations: AAD, Average Absolute Deviation; MAD, Median Absolute Deviation; RMSE, Root-Mean-Square Error.

Table 6SB. Test of the amphibole-only thermometer from Putirka (2016): expression 6. Testing model[1]: $\hat{T}_i = a + b\,T_i$

Data set[2]	*FDS*	*FDS*	*CDS2*	*CDS2*	*TDS2*	*TDS2*
Temperature range[3]	*FTR*	*CTR*	*FTR*	*CTR*	*FTR*	*CTR*
Observations	152	132	65	52	76	70
R-squared	0.31	0.44	0.29	0.33	0.49	0.60
RMSE (ºC)	53	48	46	41	47	42
AAD (ºC)	61	46	87	65	42	33
MAD (ºC)	41	33	63	53	31	29
Slope, b	0.383±0.046 t = 8.3	0.533±0.053 t = 10	0.273±0.053 t = 5.2	0.322±0.065 t = 5.0	0.559±0.066 t = 8.5	0.707±0.069 t = 10
Intercept, a	539±38 t = 14	409±44 t = 9.3	656±44 t = 15	613±55 t = 11	377±54 t = 7.0	250±57 t = 4.4

Notes: 1, non-constant regression model used when $P(>|t|) > 0$ for a parameter in model $\hat{T}_i = a + b\,T_i$. 2: CDS2, Calibration Data Set 2; FDS, Full Data Set; TDS2, Test Data Set 2. 3: CTR, Calibration Temperature Range; FTR, Full Temperature Range.
Other abbreviations: AAD, Average Absolute Deviation; MAD, Median Absolute Deviation; RMSE, Root-Mean-Square Error.

Table 7SB. Application of amphibole-plagioclase and amphibole-only thermometry to high-grade metamorphic rocks (see Appendix E for details)

Metamorphic complex	*Sample description*	*Geologicial setting*
Berit meta-ophiolite, Anatolia (SE Turkey)	*Rock types*: amphibolites, Grt-Cpx amphibolites, Pl-rich non-coronitic granulites. *Compositions used in the calculations*: magnesiohornblende, pargasite, tschermakite (Mg = 2.8-4.0 apfu); oligoclase-bytownite (p_{an} = 0.26-0.77). *Temperatures calculated* at 5-8 kbar (amphibolite and Grt-Cpx amphibolite) and 11-15 kbar (Pl-rich non coronitic granulite). *Data source*: Awalt and Whitney (2018).	Late Mesozoic to Cenozoic ophiolite fragments that mark the suture of the Arabian and Eurasian plates appear in Anatolia. The Berit meta-ophiolite represents a rare example of metamorphosed ophiolitic rocks in the SE Anatolian orogenic belt. It contains Grt (±Cpx) amphibolites, granulite-facies metagabbros, which appear as lenses in amphibolites (formed after granulites) and metaperidotites with minor metapyroxenite layers. In the Doğanşehir region, granulite-facies gabbroic rocks contain Grt+Cpx+Pl+Crn±Opx±Ky±Spr±Rt with coronitic and non-coronitic textures, and, in some samples, symplectites. *References*: Genç et al. (1993), Karaoğlan et al. (2013), Robertson et al. (2012), Awalt and Whitney (2018).
Amphibolites from the Fiskenæsset complex (SW Greenland)	*Rock types*: amphibolites, high-Cr amphibolites. *Compositions used in the calculations*: ferropargasite, magnesiohornblende, edenite (Mg = 1.7-2.6 apfu); oligoclase-bytownite (p_{an} = 0.29-0.79). *Temperatures calculated* at 7 kbar. *Data source*: Weaver et al. (1982).	The Fiskenæsset complex contains one of the best preserved Archean layered intrusions in the world. It consists of layered anorthosites, leucogabbros, gabbros, peridotites and chromitites that appear as dissected layers and lenses within amphibolites and quartzofeldspathic rocks. The complex was deformed and metamorphosed at amphibolite- to granulite- facies conditions at ca. 2.8 Ga. The amphibolites appear as up to ca. 1 km thick layers mostly limited by anorthosites, and locally by mica schists and marbles. *References*: Windley et al. (1973), Escher and Myers (1975), Rivalenti (1976), Page et al. (1980), Myers (1981), Weaver et al. (1981, 1982), Myers (1985), Ashwal et al. (1989), Riciputi et al. (1990), Peck and Valley (1996), Keulen et al. (2009), Polat et al. (2011), Polat and Longstaffe (2014), Polat (2015).
Kvalvåg granulites, Kristiansund Area, Western Gneiss Region (WGR, Norwegian Caledonides).	*Rock types*: Grt granulites. *Compositions used in the calculations*: pargasite (Mg = 2.64 apfu); andesine (p_{an} = 0.31-0.33). *Temperatures calculated* at 13.1 kbar. *Data source*: Krogh (1980).	The WGR presents the lowest exposed structural level in the southern Scandinavian Caledonides. It mostly consists of Proterozoic granitoid migmatitic and augen orthogneisses with, also common, ultramafic rocks, meta-anorthosites, mangerites, pelitic schists, quartzites, calc-silicates and marbles. Eclogites usually appear as lenticular pods or tabular layers within most of the other rock types. Based on the distribution of coesite or polycrystalline aggregates after coesite, two provinces, HP and UHP eclogites, were distinguished. In Kristiansund and other localities from the northern part of the WGR, eclogites tend to be overprinted by garnet granulite-facies assemblages, appearing trondhjemitic segregations in some eclogite bodies. *References*: Bryhni (1966), Krogh (1980, 1982), Smith (1984), Griffin et al. (1985), Mørk (1985), Jamtveit (1987), Krogh and Carswell (1995), Austrheim et al. (1997), Wain (1997), Austrheim (1998), Cuthbert et al. (2000), Austrheim et al. (2003).
Connaughton Terrane, Paleoproterozoic Rudall Complex, (Paterson Orogen, central Western Australia).	*Rock types*: Opx-Cpx amphibolites and Cpx-poor amphibolites. *Compositions used in the calculations*: pargasite, magnesiohornblende (Mg = 2.27-3.36 apfu); andesine-bytownite (p_{an} = 0.36-0.82).*Temperatures calculated* at 7 kbar. *Data source*: Smithies and Bagas (1997).	The Paterson Orogen is an arcuate, 2000 km long, belt that separates the West Australian Craton and North Australian Craton. It consists of Palaeoproterozoic to Neoproterozoic metasedimentary and meta-igneous rocks affected by the ca. 550 Myr Paterson (probably equivalent Petermann) orogeny. The Rudall Complex is exposed in the northwestern Paterson Orogen. It consists of deformed and metamorphosed Palaeoproterozoic and Mesoproterozoic sedimentary and igneous rocks. This complex has been subdivided into the Talbot, Connaughton and Tabletop terranes. The Connaughton terrane comprises a succession of mafic gneisses and schists, and paragneisses metamorphosed at the amphibolite–granulite-facies transition. It contains Opx-Cpx amphibolites, metamorphosed at granulite-facies conditions, and Cpx-poor amphibolites, generated by retrogression of the Opx-Cpx amphibolites. *References:* Williams (1990), Williams and Myers (1990), Perincek (1996), Smithies and Bagas (1997), Bagas (2004), Aitken et al. (2018).

Table 8SB. Application of amphibole-plagioclase and amphibole-only thermometry to igneous rocks (see Appendix E for details)

Igneous association	*Sample description*	*Geological setting*
Appinite suite from from the Variscan Avila batholith(Central Iberian Zone)	*Rock types*: cortlandtites. *Compositions used in the calculations*: pargasite (Mg = 3.4-3.6 apfu); andesine-labradorite (p_{an} = 0.49-0.51). *Temperatures calculated* at 3-4 kbar. *Data source*: Molina et al. (2009).	The Avila Batholith is exposed along the the axis of the Central Iberian Zone that represents the most internal paleogeographic domain of the Variscan belt of Iberia. The batholith contains 325-295 Myr plutons of strongly peraluminous granodiorites to monzongranites, blocks of migmatites (age: 352-297 Myr), minor appinitic ultramafic-mafic to intermediate stocks dated at 319-300 Myr and late Permian lamprophyre dykes. The appinites appear as enclaves included in peraluminous granitoids or intruding migmatites. The largest bodies are zoned, with cortlandtites and high-Mg gabbros at the core, and tonalites and granodiorites at the border that develop a brecciated mixed facies with mingling structures. *References:* Moreno-Ventas et al. (1995), Bea et al. (1999, 2003), Castro et al. (2003), Bea (2004), Bea et al. (2004), Montero et al. (2004a, b), Bea et al. (2006), Molina et al. (2009), Orejana et al. (2009), Scarrow et al. (2009), Bea (2010), Díaz-Alvarado et al. (2011), Villaseca et al. (2011), Molina et al. (2012), Rodríguez and Castro (2019).
Barcroft granodioritic pluton, northern White-Inyo Mountains (east-central California)	*Rock types*: gabbro-diorites, metadiorites, granodiorites. *Compositions used in the calculations*: magnesiohastingsite, magnesiohornblende (Mg = 2.6-3.3 apfu); andesine-bytownite (p_{an} = 0.32-0.83). *Temperatures calculated* at 3.8-6.6 kbar (stage 1), 1.5-6 kbar (stage 2) and 0.7-3 kbar (stage 3). *Data source*: Ernst (2002).	The White-Inyo Range lies between the Sierra Nevada fault block and the Basin and Range provinces. The 167-161 Myr Barcroft pluton is a tabular body that cuts the NNW structural trend of the White-Inyo Range and invades the Barcroft break, a NE-striking, SE-dipping high-angle reverse fault. It consists of Hbl- and Bio-rich (± relict Cpx)-bearing granodiorites, quartz gabbros and rare alaskites. Four stages of crystallization are distinguished: cumulate stage 1 at 3.8-6.6 kbar, intrusive stages 2 and 3 at 0.3-6 kbar and the deuteric stage 4 at 1-2 kbar. *References*: Ernst and Hall (1987), McKee and Conrad (1996), Ernst (2002), Ernst et al. (2003), Ernst and Rumble (2003), Michelsen (2003), Ferré et al. (2012), Ernst (2013), Chapman et al. (2015).
Bezymyannyi volcano (Kamchatka)	*Rock types*: andesites from the catastrophic 1956 eruption. *Compositions used in the calculations*: pargasite, tschermakite, magnesiohastingsite (Mg = 2.7-2.8 apfu); andesine-labradorite (p_{an} = 0.37-0.66). *Temperatures calculated* at 6-8 kbar. *Data source*: Almeev et al. (2002).	The Bezymyannyi volcano is located in the central part of the Klyuchevskaya volcanic group, southwest of Klyuchevskii volcano. It is the only active andesite volcano of this group; it experienced extremely powerful eruptions in 1956 and 1985. The andesites of Bezymyannyi volcano contain hornblende phenocrysts with opacite rims and inclusions of labradorite-andesite. *References*: Tolstykh et al. (1999), Almeev et al. (2002), Plechov et al. (2008), Ozerov et al. (2020).
Sheeted sills at Onion Valley (Mesozoic Sierra Nevada batholith)	*Rock types*: Ol hornblendites. *Compositions used in the calculations*: magnesiohastingsite, pargasite (Mg = 3.2-3.3 apfu); bytownite (p_{an} = 0.86-0.90). *Temperatures calculated* at 2-4 kbar. *Data source*: Sisson et al. (1996)	The Sierra Nevada batholith represents a very thick amalgamation of granitoid plutons dated at 248-80 Myr. It contains mostly granodiorites and granites, with minor mafic intrusions. Near Onion Valley, a mafic intrusive complex is exposed consisting of sheeted sills of Hbl gabbros to Hbl diorites, multiply-injected sills, mafic stocks and lens-shaped cumulate intrusions with layers of Hbl gabbros with minor Ol hornblendites, Pl hornblendites, and Hbl-Pl pegmatites. *References*: Bateman and Dodge (1970), Pickett and Saleeby (1993), Coleman et al. (1995), Sisson et al. (1996), Coleman and Glazner (1997), Ducea (2001), Lackey et al. (2008), Nadin and Saleeby (2008), Dumitru et al. (2010), Cecil et al. (2012), Gilbert et al. (2012).
Val Fredda Complex, Sourthern Adamello Massif (Central Alps, Italy).	*Rock types*: Hbl gabbros and diorite enclaves. *Compositions used in the calculations*: tschermakite, magnesiohornblende, actinolite (Mg = 2.5-3.5 apfu); andesine-labradorite (p_{an} = 0.42-0.62). *Temperatures calculated* at 2 kbar. *Data source*: Blundy and Holland (1990).	The Adamello batholith comprises several intrusive units dated at 42-29 Myr; it consists of tonalites, trondjhemites and granodiorites, with minor mafic and ultramafic intrusions. The Val Fredda Complex contains granodiorites, tonalites and quartz diorites intruded by mafic sheets that range from Hbl gabbros to quartz diorites in the Mt. Cadino and Hbl-phyric, Px-bearing gabbros and subordinate hornblendite blocks or bands in the Mt. Mattoni. *References:* Bianchi et al. (1970), Callegari and Dal Piaz (1973), Dupuy et al. (1982), Del Moro et al. (1983), Riklin (1983), Ulmer et al. (1983), Blundy and Holland (1990), Blundy and Sparks (1992), Callegari and Brack (2002), Mayer et al. (2003), Tiepolo et al. (2011).

References

Aitken, A., Occhipinti, S., Lindsay, M., Joly, A., Howard, H., Johnson, S., Hollis, J., Spaggiari, C., Tyler, I., and McCuaig, T. (2018) The tectonics and mineral systems of Proterozoic Western Australia: relationships with supercontinents and global secular change. Geoscience Frontiers, 9, 295–316.

Almeev, R.R., Ariskin, A.A., Ozerov, A.Y., and Kononkova, N.N. (2002) Problems of the stoichiometry and thermobarometry of magmatic amphiboles: An example of hornblende from the andesites of Bezymianny volcano, Eastern Kamchatka. Geochemistry International, 40, 723–738.

Ashwal. L.D., Jacobsen. S.B., Myers, J.S., Kalsbeck. F., and Goldstein. S.J. (1989) Sm-Nd age of the Fiskenæssct Anorthosite Complex. West Greenland. Eurth ond Planetary Science Lcaers, 91, 261-270.

Austrheim, H. (1998) The influence of fluid and deformation on metamorphism of the deep crust and consequences for the geodynamics of collision zones. In: Hacker, B., and Liou, J.G. (Eds.), When Continents Collide: Geodynamics and Geochemistry of Ultrahigh Pressure Rocks. Chapman and Hall, 297–323.

Austrheim, H.□, Corfu, F., Bryhni, I., and Andersen, T.B. (2003) The Proterozoic Hustad igneous complex: a low strain enclave with a key to the history of the Western Gneiss Region of Norway. Precambrian Research, 120, 149□–175.

Austrheim, H., Erambert, H., and Engvik, A.K. (1997) Processing of crust in the root zone of the Caledonian continental collision zone: the role of eclogitization. In: Touret, J.L.R. and Austrheim, H. (Eds.) Collision Orogens: Zones of Active Transfer Between Crust and Mantle. Tectonophysics, 273, 129–156.

Awalt, M.B., and Whitney, D.L. (2018) Petrogenesis of kyanite- and corundum-bearing mafic granulite in a meta-ophiolite, SE Turkey. Journal of Metamorphic Geology, 36, 881–904.

Bagas, L. (2004) Proterozoic evolution and tectonic setting of the northwest Paterson Orogen, Western Australia. Precambrian Research, 128, 475–496.

Bateman, P.C, and Dodge, F.C.W. (1970) Variations of major chemical constituents across the Central Sierra Nevada Batholith. Geological Society of America Bulletin, 81, 409–420.

Bea, F. (2004) La naturaleza del magmatismo de la Zona Centro Ibérica: consideraciones generales y ensayo de correlación. In: Vera, J.A. (Ed.), Geología de España. SGEIGME, Madrid, 128–133.

Bea, F. (2010) Crystallization dynamics of granite magma chambers in the absence of regional stress: multiphysics modeling with natural examples. Journal of Petrology, 51, 1541–1569.

Bea, F., Montero, P., González-Lodeiro, F., Talavera, C., Molina, J.F., Scarrow, J.H., Whitehouse, M.J., and Zinger, T.F. (2006) Zircon thermometry and U–Pb ion-microprobe dating of the gabbros and associated migmatites of the Variscan Toledo Anatectic Complex, Central Iberia. Journal of the Geological Society of London, 163, 847–855.

Bea, F., Montero, P., and Molina, J.F. (1999) Mafic precursors, peraluminous granitoids, and late lamprophyres in the Avila batholith: a model for the generation of Variscan batholiths in Iberia. The Journal of Geology, 107, 399–419.

Bea, F., Montero, P., and Zinger, T. (2003) The nature and origin of the granite source layer of Central Iberia: evidence from trace element, Sr and Nd isotopes, and zircon age patterns. The Journal of Geology, 111, 579–595.

Bea, F., Villaseca, C., and Bellido, F. (2004) El Batolito de Avila (Sistema Central Español). In: Vera J.A. (ed.) Geología de España. SGEITGE, Madrid, 101–110.

Bianchi, A., Callegari, E., and Jobstraibizer, P.G. (1970) I tipi petrografici fondimentaali del plutone dell'Adamello. Memoria degli Istituti di Geologia e Mineralogia dell'Universita di Padova, 27, 1–148.

Blundy, J.D., and Sparks, R.S.J. (1992) Petrogenesis of mafic inclusions in granitoids of the Adamello Massif, Italy. Journal of Petrology, 33, 1039–1104.

Bryhni, I. (1966) Reconnaissance studies of gneisses, ultrabasites, eclogites and anorthosites in outer Nordfjord, Western Norway. Norges Geologiske Undersøkelse Bulletin, 241, 1–68.

Callegari, E., and Brack, P. (2002) Geological map of the Tertiary Adamello batholith (Northern Italy). Explanatory notes and legend. Memorie di Scienze Geologiche 54, 19–49.

Callegari, E., and Dal Piaz, G.B. (1973) Field relationships between the main igneous masses of the Adamello Intrusive Massif (N. Italy). Memorie degli Istituti Geologia e Mineralogia dell'Università di Padova, 24, 1–38.

Castro, A., Corretge, L.G., De la Rosa, J.D., Fernandez, C., Lopez, S., Garcia-Moreno, O., and Chacon, H. (2003) The appinite–migmatite complex of Sanabria, NW Iberian massif, Spain. Journal of Petrology, 44, 1309–1344.

Cecil, M.R., Rothberg, G.L., Ducea, M.N., Saleeby, J.B., and Gehrels, G.E. (2012) Magmatic growth and batholithic root development in the northern Sierra Nevada, California. Geosphere, 8, 592–606.

Chapman, A.D., Ernst, W.G., Gottlieb, E., Powerman, V., and Metzger, E.P. (2015) Detrital zircon geochronology of Neoproterozoic–Lower Cambrian passive-margin strata of the White-Inyo Range, east-central California: Implications for the Mojave–Snow Lake fault hypothesis. Geological Society of America Bulletin, B31142-1, doi: 10.1130/B31142.1.

Coleman, D.S., and Glazner, A.F. (1997) The Sierra Crest Magmatic Event: rapid formation of juvenile crust during the Late Cretaceous in California. International Geology Review, 39, 768–787.

Coleman, D.S., Glazner, A.F., Miller, J.S., Bradford, K.J., Frost, T.P., Joye, J.L., and Bachl, C.A. (1995) Exposure of a late Cretaceous layered mafic-felsic magma system in the central Sierra Nevada batholith, California. Contributions to Mineralogy and Petrology, 120, 129–136.

Cuthbert, S.J., Carswell, D.A., Krogh-Ravna, E.J., and Wain A. (2000) Eclogites and eclogites in the Western Gneiss Region, Norwegian Caledonides. Lithos, 52, 165–195.

Del Moro, A., Ferrara, G.,Tonarini, S., and Callegari, E. (1983) Rb-Sr systematics on the rocks from the Adamello batholith (Southern Alps). Memorie della Società Geologica Italiana 26, 261–284.

Díaz-Alvarado, J., Castro, A., Fernández, C., and Moreno-Ventas, I. (2011) Assessing bulk assimilation in cordierite-bearing granitoids from the Central System Batholith, Spain; experimental, geochemical and geochronological constraints. Journal of Petrology, 52, 223–256.

Ducea, M.N. (2001) The California arc: Thick granitic batholiths, eclogitic residues, lithospheric-scale thrusting, and magmatic flare-ups. G.S.A. Today, 11, 4–10.

Dumitru, T.A., Wakabayashi, J., Wright, J.E., and Wooden, J.L. (2010) Early Cretaceous transition from nonaccretionary behavior to strongly accretionary behavior within the Franciscan subduction complex. Tectonics, 29, TC5001.

Dupuy, C., Dostal, J., and Fratta, M. (1982) Geochemistry of the Adamello massif (Northern Italy). Contributions to Mineralogy and Petrology, 80, 41-48.

Ernst, W.G. (2002) Paragenesis and thermobarometry of Ca-amphiboles in the Barcroft granodioritic pluton, central White Mountains, eastern California. American Mineralogist, 87, 478–490.

Ernst, W.G. (2013) Petrogenesis of the Barcroft pluton, northern White-Inyo Mountains, east-central California. Contributions to Mineralogy and Petrology, 165, 419–435.

Ernst, W.G., Coleman, D.S., and Van de Ven, C.M. (2003) Petrochemistry of granitic rocks in the Mount Barcroft area. Implications for arc evolution, central White Mountains, easternmost California. Geological Society of America Bulletin, 115, 499–512.

Ernst, W.G., and Hall, C.A. (1987) Geology of the north Barcroft-Blanco Mountain Area, Eastern California. Geological Society of America Map and Chart Series MCH006.

Ernst, W.G., and Rumble, D. (2003) Oxygen isotopic study of Late Mesozoic cooling of the Mount Barcroft area, central White Mountains, eastern California. Contributions to Mineralogy and Petrology, 144, 639–651.

Escher, J.C., and Myers, J.S. (1975) New evidence concerning the original relationships of early Precambrian volcanics and anorthosites in the Fiskenæsset region, southern West Greenland: Grønlands Geologiske Undersøgelse Rapport, 75, 72–76.

Ferré, E.C., Michelsen, K.J., Ernst, W.G., Boyd, J.D., and Canon-Tapia, E. (2012) Vertical zonation of the Barcroft granodiorite, White Mountains, California: implications for magmatic processes. American Mineralogist, 97, 1049–1059.

Genç, Ş. C., Yiğitbaş, E., and Yılmaz, Y. (1993) Geology of the Berit metaophiolite. In A. Suat Erk geology symposium, expanded abstracts. Ankara University Geology Department, Ankara. 37–52.

Gilbert, H., Yang, Y., Forsyth, D.W., Jones, C.H., Owens, T.J., Zandt, G., and Stachnik, J.C. (2012) Imaging lithospheric foundering in the structure of the Sierra Nevada. Geosphere, 8, 1310–1330.

Griffin, W.L., Austrheim, H., Brastad, K., Bryhni, I., Krill, A.G., Krogh, E.J., Mørk, M.B.E., Qvale, H., Tørudbakken, B. (1985) High-pressure metamorphism in the Scandinavian Caledonides. In: Gee, D.G., and Sturt, B.A. (Eds.), The Caledonide Orogen — Scandinavia and Related Areas. Wiley, Chichester, 783–801.

Jamtveit, B. (1987) Metamorphic evolution of the Eiksunddal eclogite Complex, Western Norway, and some tectonic implications. Contributions to Mineralogy and Petrology, 95, 82–99.

Karaoğlan, F., Parlak, O., Robertson, A.H.F., Thöni, M., Klötzli, U., Koller, F., and Okay, A.I. (2013) Evidence of Eocene high-temperature/high-pressure metamorphism of ophiolitic rocks and (Doğanşehir area, SE Anatolia). In Robertson, A.H.F., Parlak, O., and Ünlügenç, U.C. (Eds.), Geological development of Anatolia and the Easternmost Mediterranean Region. London: Geological Society, London, Special Publications, 372, 249–272.

Keulen, N., Schersten, A., Schumacher, J.C., Næraa, T., and Windley, B.F. (2009) Geological observations in the southern West Greenland basement from Ameralik to Frederikshab Isblink in 2008. Geological Survey of Denmark and Greenland Bulletin, 17, 49–52.

Krogh, E.J. (1980) Compatible P-T conditions for eclogites and surrounding gneisscs in the Kristiansund area, western Norway. Contributions to Mineralogy and Petrology, 75, 387–393.

Krogh, E.J. (1982) Metamorphic evolution of Norwegian country-rock eclogites, as deduced from mineral inclusions and compositional zoning in garnets. Lithos 15, 305–321.

Krogh, E.J., and Carswell, D.A. (1995) HP and UHP eclogites and garnet peridotites in the Scandinavian Caledonides. In: Coleman, R.G., Wang, X. Eds.., Ultrahigh Pressure Metamorphism. Cambridge Univ. Press, pp. 244–298.

Lackey, J.S., Valley, J.W., Chen, J.H., and Stockli, D.F. (2008) Dynamic magma systems, crustal recycling, and alteration in the central Sierra Nevada batholith: the oxygen isotope record. Journal of Petrology, 49, 1397–1426.

Mayer, A., Cortiana, G., Dal Piaz, G.V., Deloule, E., De Pieri, R., and Jobstraibizer, P. (2003). U-Pb single zircon ages of the Adamello batholith, Southern Alps. Memorie della Società Geologica 55, 151–167.

McKee, E.H., and Conrad, J.E. (1996) A tale of 10 plutons—Revisited: Age of granitic rocks in the White Mountains, California and Nevada. Geological Society of America Bulletin, 108, 1515–1527.

Michelsen, K.J. (2003) Heterogeneous internal fabric of the Mount Barcroft pluton, White Mountains, of eastern California: an anisotropy of magnetic susceptibility study, 115 p., M.Sc. thesis, Virginia Tech, Blacksburg.

Molina, J.F., Montero, P., Bea, F., and Scarrow, J.H. (2012) Anomalous xenocryst dispersion during tonalite–granodiorite crystal mush hybridization in the mid crust: Mineralogical and geochemical evidence from Variscan appinites (Avila Batholith, Central Iberia). Lithos, 153, 224–242.

Montero, P., Bea, F., and Zinger, T. (2004a) Edad $^{207}Pb/^{206}Pb$ en cristal único de circón de las rocas máficas y ultramáficas del sector de Gredos, Batolito de Avila (Iberia Central). Revista de la Sociedad Geológica de España, 17, 157–165.

Montero, P., Bea, F., Zinger, T.F., Scarrow, J.H., Molina, J.F., and Whitehouse, M.J. (2004b) 55 million years of continuous anatexis in Central Iberia: single zircon dating of the Peña Negra Complex. Journal of the Geological Society of London, 161, 255–264.

Moreno-Ventas, I., Rogers, G., and Castro, A. (1995) The role of hybridization in the genesis of Hercynian granitoids in the Gredos Massif, Spain: inferences from Sr–Nd isotopes. Contributions to Mineralogy and Petrology, 120, 137–149.

Mørk, M.B.E. (1985) A gabbro to eclogite transition on Flemsøy, Sunnmøre, west Norway. Chemical Geology, 50, 283–310.

Myers, J.S. (1981) The Fiskenæsset anorthosite complex —A stratigraphic key to the tectonic evolution of the western Greenland gneiss complex 3000–2800 m.y. ago. Geological Society of Australia Special Publication, 7, 351–361.

Myers, J.S. (1985) Stratigraphy and structure of the Fiskenæsset Complex, southern West Greenland. Grønlands Geologiske Undersøgelse Bulletin, 150, 72 p.

Nadin, E.S., and Saleeby, J.B. (2008) Disruption of regional primary structure of the Sierra Nevada batholith by the Kern Canyon fault system, California, in Wright, J.E., and Shervais, J.W., eds., Ophiolites, Arcs, and Batholiths: A Tribute to Cliff Hopson: Geological Society of America Special Paper, 438, 429–454.

Orejana, D., Villaseca, C., Pérez–Soba, C., López–García, J.A., and Billström, K. (2009) The Variscan gabbros from the Spanish Central System: A case for crustal recycling in the sub-continental lithospheric mantle? Lithos, 110, 262–276.

Ozerov, A.Y., Girina, O.A., Zharinov, N.A., Belousov, A.B., and Demyanchuk, Y.V. (2020) Eruptions in the Northern Group of Volcanoes, in Kamchatka, during the Early 21st Century. Journal of Volcanology and Seismology, 14, 1–17.

Page, N.J., Myers, J.S., Haffty, J., Simon, F.O., and Aruscavage, P.J. (1980) Platinum, palladium and rhodium in the Fiskenæsset complex, southern west Greenland. Economic Geology, 75, 907–915.

Patiño-Douce, A.E., and Beard, J.S. (1995) Dehydration-melting of biotite gneiss and quartz amphibolite from 3 to 15 kbar. Journal of Petrology, 36, 707–738.

Peck, W.H., and Valley, J.W. (1996) The Fiskenæsset Anorthosite Complex: stable isotope evidence for shallow emplacement into Archean oceanic crust. Geology, 24, 523–526.

Perincek, D. (1996) The age of the Neoproterozoic–Palaeozoic sediments within the Officer Basin of the Centralian Super-Basin can be constrained by major sequence-boundary unconformities. APPEA Journal, 36, 350–368.

Pickett, D.A., and Saleeby, J.B. (1993) Thermobarometric constraints on the depth of exposure and conditions of plutonism and metamorphism at deep levels of the Sierra Nevada batholith, Tehachapi Mountains, California. Journal of Geophysical Research. Solid Earth, 98, 609–629.

Plechov, P.Y., Tsai A.E., Shcherbakov V.D. and Dirksen, O.V. (2008) Opacitization conditions of hornblende in Bezymyannyi Volcano andesites (March 30, 1956 eruption). Petrology, 16, 19–35.

Polat, A. (2015) A review of structural patterns and melting processes in the Archean craton of West Greenland: Evidence for crustal growth at convergent plate margins as opposed to non-uniformitarian models. Tectonophysics, 662, 67-94.

Polat, A., Fryer, B., Appel, P.W.U., Kalvig, P., Kerrich, R., Dilek, Y., and Yang, Z. (2011) Geochemistry of anorthositic differentiated sills in the Archean (~2970 Ma) Fiskenæsset Complex, SW Greenland: Implications for parental magma compositions, geodynamic setting, and secular heat flow in arcs. Lithos 123, 50–72.

Polat, A., and Longstaffe, F.J. (2014) A juvenile oceanic island arc origin for the Archean (ca. 2.97 Ga) Fiskenæsset Anorthosite Complex, southwestern Greenland: Evidence from oxygen isotopes. Earth and Planetary Science Letters, 396, 252–266.

Riciputi, L.R., Valley, J.W., and McGregor, V.R. (1990) Conditions of Archean granulite metamorphism in the Godthåb–Fiskenæsset region, southern West Greenland. Journal of Metamorphic Geology, 8, 171–190.

Riklin, K. (1983) Contact metamorphism of the Permian red sandstones in the Adamello area. Memorie della Società Geologica Italiana, 26, 159–169.

Rivalenti, G. (1976) Geochemistry of metavolcanic amphibolites from south-west Greenland, in Windley, B.F. (ed.) The early history of the Earth: London, John Wiley and Sons, p. 213–223.

Robertson, A.H.F., Parlak, O., and Ustaömer, T. (2012) Overview of the Palaeozoic-Neogene evolution of Neotethys in the Eastern Mediterranean region (southern Turkey, Cyprus, Syria). Petroleum Geoscience, 18, 381–404.

Rodríguez, C., and Castro, A. (2019) Origins of mafic microgranular enclaves and enclave swarms in granites: field and geochemical relations. Geological Society of America Bulletin, 131, 635–660.

Scarrow, J.H., Molina, J.F., Bea, F., and Montero, P. (2009) Within-plate calc-alkaline rocks: insights from alkaline mafic magma-peraluminous crustal melt hybrid appinites of the Central Iberian Variscan continental collision. Lithos, 110, 50–64.

Sisson, T.W., Grove, T.L., and Coleman, D.S. (1996) Hornblende gabbro sill complex at Onion Valley, California, and a mixing origin for the Sierra-Nevada batholith. Contributions to Mineralogy and Petrology, 126, 81–108.

Smith, D.C. (1984) Coesite in clinopyroxene in the Caledonides and its implication for geodynamics. Nature 310, 641–644.

Smithies, R.H., and Bagas, L. (1997) High-pressure amphibolite–granulite facies metamorphism in the Paleoproterozoic Rudall Complex, central Western Australia. Precambrian Research, 83, 243–265.

Tiepolo, M., Tribuzio, R., and Langone, A. (2011) High-Mg andesite petrogenesis by amphibole crystallization and ultramafic crust assimilation: evidence from Adamello hornblendites (Central Alps, Italy). Journal of Petrology, 52, 1011–1045.

Tolstykh, M.L., Naumov , V.B., Bogoyavlenskaya, G.E., and Kononkova, N.N. (1999) The Role of Andesitic–Dacitic–Rhyolitic Melts in the Crystallization of Phenocrysts in Andesite of Bezymyannyi Volcano, Kamchatka. Geochemistry International, 37, 11–20.

Ulmer, P., Callegari, E., and Sonderegger, U.C. (1983) Genesis of the mafic and ultramafic rocks and their genetic relations to the tonalitic-trondjemitic granitoids of the southern part of the Adamello batholith (Northern Italy). Memorie della Società Geologica Italiana, 26, 171–222.

Villaseca, C., Orejana, D., Belousova, E.A., Armstrong, R.A., Pérez-Soba C., and Jeffries T.E. (2011) U-Pb isotopic ages and Hf isotope com- position of zircons in Variscan gabbros from central Spain: evidence of variable crustal contamination. Mineralogy and Petrology, 101, 151–167.

Wain, A.L. (1997) New evidence for coesite in eclogite and gneisses: defining an ultrahigh pressure province in the Western Gneiss Region of Norway. Geology, 25, 927–930.

Weaver, B.L., Tarney, J., and Windley, B.F. (1981) Geochemistry and petrogenesis of the Fiskenæsset anorthosite complex, southern West Greenland: Nature of the parent magma: Geochimica et Cosmochimica Acta, 45, 711–725.

Weaver, B.L., Tarney, J., Windley, B., and Leake, B.E. (1982) Geochemistry and petrogenesis of Archean metavolcanic amphibolites from Fiskenæsset, S.W. Greenland. Geochimica et Cosmochimica Acta, 46, 2203–2215.

Williams, I.R. (1990) Yeneena Basin. In: Geology and Mineral Resources of Western Australia. Western Australia Geological Survey, Memoir, 3, 277–282.

Williams, I.R., and Myers, J.S. (1990) Paterson Orogen. In: Geology and Mineral Resources of Western Australia. Western Australia Geological Survey, Memoir, 3, 282–283.

Windley, B.F., Herd, R.K., and Bowden, A.A. (1973) The Fiskenæsset Complex, West Greenland: Grønlands Geologiske Undersøgelse Bulletin, 106, 80 p.